Molecular Dynamics in Paramagnetic Materials as Studied by Magic-Angle Spinning ^{2}H NMR Spectra

Motohiro Mizuno,*,† You Suzuki,† Kazunaka Endo,† Miwa Murakami,‡ Masataka Tansho,‡ and Tadashi Shimizu‡

Department of Chemistry, Graduate School of Natural Science and Technology, Kanazawa University, Kanazawa, Ishikawa 920-1192, Japan, and National Institute for Materials Science, 3-13 Sakura, Tsukuba, Ibaraki 305-0003, Japan

Received: July 11, 2007; In Final Form: September 24, 2007

A magic-angle spinning (MAS) ^{2}H NMR experiment was applied to study the molecular motion in paramagnetic compounds. The temperature dependences of ^{2}H MAS NMR spectra were measured for paramagnetic $[M(H_2O)_6][SiF_6]$ ($M = Ni^{2+}$, Mn^{2+}, Co^{2+}) and diamagnetic $[Zn(H_2O)_6][SiF_6]$. The paramagnetic compounds exhibited an asymmetric line shape in ^{2}H MAS NMR spectra because of the electron−nuclear dipolar coupling. The drastic changes in the shape of spinning sideband patterns and in the line width of spinning sidebands due to the 180° flip of water molecules and the reorientation of $[M(H_2O)_6]^{2+}$ about its C_3 axis were observed. In the paramagnetic compounds, paramagnetic spin−spin relaxation and anisotropic g-factor result in additional linebroadening of each of the spinning sidebands. The spectral simulation of MAS ^{2}H NMR, including the effects of paramagnetic shift and anisotropic spin−spin relaxation due to electron−nuclear dipolar coupling and anisotropic g-factor, was performed for several molecular motions. Information about molecular motions in the dynamic range of $10^2\ s^{-1} \le k \le 10^8\ s^{-1}$ can be obtained for the paramagnetic compounds from the analysis of ^{2}H MAS NMR spectra when these paramagnetic effects are taken into account.

1. Introduction

Solid-state ^{2}H NMR spectroscopy has developed into a powerful tool in studies of local molecular geometry and dynamics in solids.[1−3] The information of the molecular motion in the wide dynamic range (typically $10^{-2}\sim10^{10}\ s^{-1}$) can be obtained using the spin−lattice relaxation time (T_1), one-dimensional spectra, and two-dimensional exchange spectra for diamagnetic compounds. For paramagnetic substances, because of the fast spin−lattice relaxation due to the interaction between the unpaired electron spin and the resonant nuclei, the use of T_1 and two-dimensional exchange spectra for the study of molecular dynamics is difficult. So, the line shape analysis of the one-dimensional NMR spectra becomes very important for studying molecular dynamics in paramagnetic compounds. The line shape of a ^{2}H NMR spectrum depends on the anisotropic interactions, such as nuclear quadrupole interaction, chemical shift, and dipolar interaction, and is affected by the molecular motion. The line shape of a broadline ^{2}H NMR spectrum is sensitive to the molecular motion in the dynamic range of $10^3\ s^{-1} \le k \le 10^7\ s^{-1}$.[2−10] Since the ordinary quadrupole-echo sequence refocuses only dephasing due to the quadrupole interaction, the distortion of the line shape is caused by the paramagnetic shift in the measurements of broadline ^{2}H NMR spectra of paramagnetic compounds. Two- or four-pulse sequences which remove the distortion of a spectrum because of the paramagnetic shift have been proposed.[11,12] The simulation method for the ^{2}H NMR broadline spectrum of paramagnetic compounds obtained by these pulse sequences has been developed for the study of molecular dynamics in paramagnetic compounds.[2,13−19]

^{2}H magic-angle spinning (MAS) NMR spectra with spinning sidebands have also been shown to be sensitive to molecular motions with the rates, $10^2\ s^{-1} \le k \le 10^3\ s^{-1}$ and $10^7\ s^{-1} \le k \le 10^9\ s^{-1}$, which are almost undetectable in the ^{2}H NMR broadline spectra.[25−27] Therefore, information of molecular motions in a wide dynamic range can be obtaind by the combined use of ^{2}H NMR MAS and broadline spectra. The theory for the analysis of MAS NMR spectral line shape in the presence of a molecular motion has been developed using the Floquet formalism and a stepwise calculation of the time evolution of the magnetization for diamagnetic compounds.[20−27] For the measurements of ^{2}H MAS NMR spectra in paramagnetic compounds, the dephasings of magnetization due to the quadrupole interaction and the dipolar interaction between the deuteron and the paramagnetic ions are refocused not by the refocus pulse but rather by MAS. This removes the difficulty in analysis caused by the effects of finite pulse width on the spectra and allows one to obtain reliable information about the local structure in paramagnetic compounds. Thus, use of MAS NMR spectra is especially effective for the analysis of paramagnetic compounds.

In the present work, the effects of molecular motion such as a 180° flip of water molecules and reorientation of $[M(H_2O)_6]^{2+}$ about its C_3 axis on the ^{2}H MAS NMR spectra were investigated for paramagnetic $[M(H_2O)_6][SiF_6]$ ($M = Ni^{2+}$, Mn^{2+}, Co^{2+}) and diamagnetic $[Zn(H_2O)_6][SiF_6]$. The dynamics of molecules and electron spin in these compounds have been investigated by the ^{2}H NMR spectrum of a single crystal, the ^{2}H NMR broadline spectrum, and T_1 of the powder samples.[14−19,28] In the ^{2}H MAS NMR spectra of paramagnetic compounds, the dipolar interaction between the deuteron and the paramagnetic ions causes an

* Corresponding author. Fax: +81-76-264-5742. E-mail: mizuno@wriron1.s.kanazawa-u.ac.jp.
† Kanazawa University.
‡ National Institute for Materials Science.

10.1021/jp075405l CCC: $37.00
Published on Web 11/21/2007

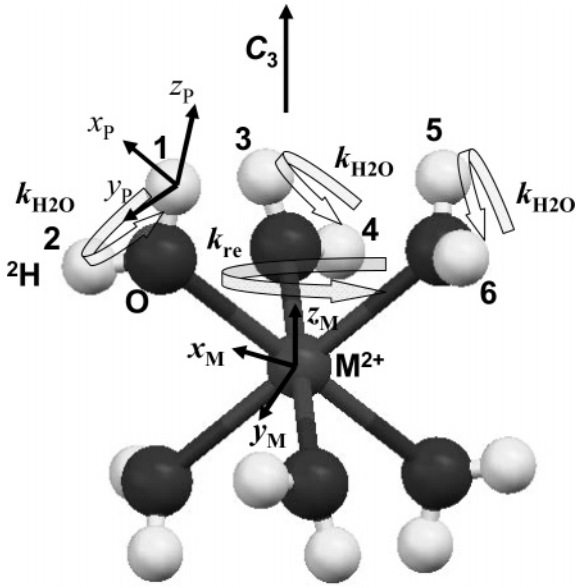

Figure 1. Six-site jump of deuterons caused by the 180° flip of water molecules and the three-site jump of $[M(H_2O)_6]^{2+}$ about the C_3 axis.

TABLE 1: Magnetic and Geometric Parameters of $[M(H_2O)_6][SiF_6]$ Used for Spectral Simulation

metal ion M^{2+}	spin state S	g-factor $g_{\parallel}$, $g_{\perp}$	deuterons	nearest M−D distance (pm)	Euler angles (degrees) α_q	β_q	γ_q
Zn^{2+}			D1		0.0	166.8	346.0
			D2		166.6	85.5	3.2
Ni^{2+}	1	2.26	D1	257	0.0	168.3	349.2
			D2	244	169.6	82.2	2.2
Mn^{2+}	5/2	2.00	D1	276	0.0	168.0	49.7
			D2	282	235.3	78.7	350.7
Co^{2+}	1/2	5.90, 5.00	D1	266	0.0	165.8	320.1
			D2	256	142.0	82.6	9.1

asymmetric spinning sideband pattern. Previously, the line shape of ^{2}H MAS NMR spectra in paramagnetic compounds had been investigated only in slow and fast limit motion regimes.[29,30] We discuss the effects of intermediate time scale molecular motions on ^{2}H MAS NMR spectra in paramagnetic compounds. For the ^{2}H MAS NMR spectra of paramagnetic compounds, the anisotropy of the g-factor of paramagnetic ions and the fast spin−spin relaxation due to the dipolar interaction between the deuteron and the paramagnetic ions, as well as molecular motion, affect largely the line width of the spinning sideband. The ^{2}H MAS NMR spectral simulation, including the effects of paramagnetic shift, anisotropic g-factor, and anisotropic spin−spin relaxation due to the dipolar interaction between the deuteron and the paramagnetic ions in the presence of the molecular motion, was performed using not only the nearest paramagnetic ion but also the distant ones. When the broadening of the linewidths are caused by the fast paramagnetic transverse relaxation, the imaginary part of the spectral density gives rise to the shift in the resonance frequency, often referred to as the dynamic frequency shift (DFS).[31] The effects of DFS to the ^{2}H MAS NMR spectrum were also investigated. A point dipole model was used for the calculation of the dipolar interaction between the deuteron and the paramagnetic ions. The simulation spectrum was obtained by stepwise integration for the equation of the time evolution of magnetization. Application of the proposed simulation method to the analysis of molecular dynamics in paramagnetic samples is discussed by comparing the results of ^{2}H NMR MAS spectra and broadline spectra for paramagnetic $[M(H_2O)_6][SiF_6]$ ($M = Ni^{2+}$, Mn^{2+}, Co^{2+}) and diamagnetic $[Zn(H_2O)_6][SiF_6]$.

2. Experimental Section

The deuterated sample was obtained by repeated recrystallization from heavy water. The ^{2}H NMR experiments of $[M(H_2O)_6][SiF_6]$ ($M = Zn^{2+}$, Ni^{2+}, Co^{2+}) were carried out using a Chemagnetics CMX-300 spectrometer at 45.826 MHz with a 7.5 mm diameter zirconia rotor. The ^{2}H NMR experiments of $[Mn(H_2O)_6][SiF_6]$ were carried out using a JEOL JNM-ECA500 spectrometer at 76.777 MHz with a 4.0 mm diameter zirconia rotor. 90°−τ−acq pulse sequence was used. τ was synchronized with MAS speed, and signal was collected beginning at the top of the first rotational echo. The 90° pulse width was 3.4 and 2.4 μs for the measurements of $[M(H_2O)_6][SiF_6]$ ($M = Zn^{2+}$, Ni^{2+}, Co^{2+}) and $[Mn(H_2O)_6][SiF_6]$, respectively. After coarse adjustment of the magic angle using a KBr sample, fine adjustments were made using the line width of the spinning sideband of the ^{2}H MAS NMR spectrum of $[Zn(H_2O)_6][SiF_6]$ at room temperature (0.32 kHz). The measurements of the ^{2}H MAS NMR spectra were performed from room temperature to the decomposition point of samples. The simulation of the ^{2}H MAS NMR spectrum was performed by homemade Fortran programs according to eqs 1−22 using double precision. The numerical diagonalization of a complex, non-Hermitian matrix A in eq 17 was performed using the Eispack implementation of the QR algorithm.[32]

3. Theory and Simulations

The calculations in the present work were performed by considering the ^{2}H NMR frequency and the spin−spin relaxation rate at each deuteron site and the jump frequency of deuterons between the sites. The ^{2}H NMR frequency at site i ($\omega_i(t)$) for a sample under MAS is written as

$$\omega_i(t) = \pm\omega_{Q_i}(t) - \sum_j \omega_{Pij}(t) + \omega_{CS_i} \tag{1}$$

where ω_{CS_i} is the time-independent contribution of Fermi's contact shift. $\omega_{Qi}(t)$ and $\omega_{P_{ij}}(t)$ are the time-dependent contributions of the quadrupole interaction and the dipolar interaction between ^{2}H nucleus and the jth paramagnetic ion, which are written by the second-order Wigner rotation matrix $D^{(2)*}_{nm}(\Omega)$ as[2,5,15,17,19,33]

$$\omega_{Qi}(t) = \sqrt{\frac{3}{2}} \sum_{n,k,m=-2}^{2} D^{(2)*}_{0n}(0, -\theta_m, \omega_r t) D^{(2)*}_{nk}(\alpha, \beta, \gamma) \times D^{(2)*}_{km}(\alpha_{qi}, \beta_{qi}, \gamma_{qi}) T^{(2)}_{mQ} \tag{2}$$

$$\omega_{P_{ij}}(t) = \sum_{n,k=-2}^{2} D^{(2)*}_{0n}(0, -\theta_m, \omega_r t) D^{(2)*}_{nk}(\alpha, \beta, \gamma) \times D^{(2)*}_{k0}(\alpha_{pij}, \beta_{pij}, \gamma_{pij}) \omega_{D_{ij}}(t) \tag{3}$$

$$T^{(2)}_{0Q} = \sqrt{\frac{3}{8}} \frac{e^2 Qq}{\hbar} T_{\pm 2Q}{}^{(2)} = \frac{\eta}{4} \frac{e^2 Qq}{\hbar} \tag{4}$$

$$\omega_{Dij}(t) = \left(\frac{\mu_0}{4\pi}\right) \frac{2\gamma_D B_0 g_j^2(t) \mu_B^2}{3k_B T r_{ij}^3} S(S+1) \tag{5}$$

$$g_j^2(t) = g_{\mathrm{iso}_j}^2 + \sum_{n,k,m=-2}^{2} D_{0n}^{(2)*}(0, -\theta_m, \omega_r t) D_{nk}^{(2)*}(\alpha, \beta, \gamma) \times D_{km}^{(2)*}(\alpha_{gj}, \beta_{gj}, \gamma_{gj}) T_{mg_j}^{(2)} \quad (6)$$

$$T_{0g_j}^{(2)} = \sqrt{\frac{2}{3}}\left(g_{zz_j}^2 - \frac{1}{2}(g_{xx_j}^2 + g_{yy_j}^2)\right)$$

$$T_{\pm 2 g_i}^{(2)} = \frac{1}{2}(g_{yy_j}^2 - g_{xx_j}^2) \quad (7)$$

$$g_{\mathrm{iso}_j}^2 = \frac{g_{xx_j}^2 + g_{yy_j}^2 + g_{zz_j}^2}{3} \quad (8)$$

where θ_m ($= \cos^{-1} 1/\sqrt{3}$) is the magic angle and ω_r is the sample spinning speed. (α_{qi}, β_{qi}, γ_{qi}), (α_{pij}, β_{pij}, γ_{pij}), (α_{gj}, β_{gj}, γ_{gj}), and (α, β, γ) are the Euler angles for the transformation from the molecular axes to the principal axes of the electric field gradient (EFG) tensor, from the molecular axes to the principal axes of the dipolar interaction between ^{2}H nucleus and the jth paramagnetic ion, from the molecular axes to the principal axes of the g-tensor of the jth paramagnetic ion and from the rotor axes to the molecular axes, respectively. $e^2Qq/\hbar$ and η are the quadrupole coupling parameters. The spin−spin relaxation rate R_{2p}^i due to the dipolar interaction between the ^{2}H nucleus at site i and the paramagnetic ions is written as[19]

$$R_{2p}^i(t) = \frac{4}{3}\left(\frac{\mu_0}{4\pi}\right)^2 \gamma_D^2 \mu_B^2 S(S+1) \sum_j g_j^2(t) \times \left\{\frac{1}{6}\left|A_{20}^{ij}(t)\right|^2 \left(4\tau_e + \frac{\tau_e}{1 + (\omega_N - \omega_e)^2 \tau_e^2}\right) + \frac{1}{2}\left|A_{21}^{ij}(t)\right|^2 \left(\frac{2\tau_e}{1 + \omega_e^2 \tau_e^2} + \frac{\tau_e}{1 + \omega_N^2 \tau_e^2}\right) + \left|A_{22}^{ij}(t)\right|^2 \frac{\tau_e}{1 + (\omega_N + \omega_e)^2 \tau_e^2}\right\} \quad (9)$$

where ω_N and ω_e are angular NMR and ESR frequencies,

$$A_{2m}^{ij}(t) = \sum_{n,k=-2}^{2} D_{mn}^{(2)*}(0, -\theta_m, \omega_r t) D_{nk}^{(2)*}(\alpha, \beta, \gamma) \times D_{k0}^{(2)*}(\alpha_{pij}, \beta_{pij}, \gamma_{pij}) T_{0D}^{ij} \quad (10)$$

$$T_{0D}^{ij} = \sqrt{\frac{3}{2}}\, r_{ij}^{-3} \quad (11)$$

respectively. τ_e is the correlation time of the electron spin. The time evolution of the magnetization $M(t)$ is represented by[20−22,25,27]

$$M(t) = \hat{\mathbf{L}}(t) M(0) \quad (12)$$

$$\hat{\mathbf{L}}(t) = T \exp\left[\int_0^t \hat{\mathbf{A}}(t')\, \mathrm{d}t'\right] \quad (13)$$

where T is the Dyson time-ordering operator. For the exchange between N sites, $\hat{\mathbf{A}}(t)$ is an $N \times N$ dimensional matrix with the elements

$$\begin{cases} i\omega_i(t) - k_{ii} - \mathrm{R}_{2p}^i(t) & \text{on the diagonal} \\ k_{ij} & \text{off the diagonal} \end{cases} \quad (14)$$

$$k_{ii} = \sum_{j \neq i} k_{ij} \quad (15)$$

where k_{ij} is the jumping rate between site i and j. Here, we consider equal time increments Δt such that $t = n\Delta t$. By assuming time-independent A(t) for a short period of time Δt, $L(t)$ is written as[24,25]

$$\hat{\mathbf{L}}(t) = \hat{\mathbf{L}}(n\Delta t) = T \prod_{n'=1}^{n} \hat{\mathbf{S}}((n'-1)\Delta t) \times \exp[\hat{\Lambda}((n'-1)\Delta t)\Delta t] \hat{\mathbf{S}}((n'-1)\Delta t)^{-1} \quad (16)$$

$$\hat{\Lambda}((n'-1)\Delta t) = \hat{\mathbf{S}}((n'-1)\Delta t)^{-1} \hat{\mathbf{A}}((n'-1)\Delta t) \hat{\mathbf{S}}((n'-1)\Delta t) \quad (17)$$

where $\hat{\mathbf{S}}((n'-1)\Delta t)$ is the matrix which transforms $\hat{\mathbf{A}}((n'-1)\Delta t)$ into a diagonal matrix $\hat{\mathbf{\Lambda}}((n'-1)\Delta t)$. When one rotor period is divided into n_{rot} equal periods Δt, the following relation is obtained

$$\exp[\hat{\mathbf{A}}((n_{\mathrm{rot}} + 1)\Delta t)\Delta t] = \exp[\hat{\mathbf{A}}(\Delta t)\Delta t] \quad (18)$$

Once $\hat{\mathbf{\Lambda}}((n'-1)\Delta t)$, $\hat{\mathbf{S}}((n'-1)\Delta t)$, and $\hat{\mathbf{L}}(t)$ are estimated over one rotor period, $\hat{\mathbf{L}}(t)$ at subsequent times are calculated using these matrices and eq 18. The NMR signal is given by

$$G(\alpha, \beta, \gamma, t) = \mathbf{1} \cdot \hat{\mathbf{B}} \cdot \hat{\mathbf{L}}(t) \cdot M(0) \quad (19)$$

where $\mathbf{1}$ is a vector written by $\mathbf{1} = (1, 1, 1, 1, 1, 1)$. The effect of the finite 90° pulse width on the spectrum is simply considered using $\hat{\mathbf{B}}$ which is the diagonal matrix with

$$B_i = \sin(\pi K_i/2)/K_i \qquad K_i^2 = 1 + (\Omega_i/\pi)^2 \quad (20)$$

$$\Omega_i = \int_0^{t_p} \Omega_i(t)\, \mathrm{d}t \quad (21)$$

where t_p and $\Omega_i(t)$ represent the 90° pulse width and the imaginary part of the eigenvalue of the matrix $\hat{\mathbf{A}}(t)$.[34,35] The signal of a powder sample is given by

$$G(t) = \int_0^{2\pi} \int_0^{\pi} \int_0^{2\pi} G(\alpha, \beta, \gamma, t) \sin\beta\, \mathrm{d}\alpha\, \mathrm{d}\beta\, \mathrm{d}\gamma \quad (22)$$

The spectrum can be obtained by a Fourier transform of $G(t)$.

For the spectral simulation including the motion of $[M(H_2O)_6]^{2+}$, the z axis of EFG tensor (z_P) is assumed to be parallel to the direction of the O−D bond, and the six-site jump model with the rates k_{H_2O} and k_{re} as shown in Figure 1 is used. The z and y axis of the molecular axes (z_M, y_M) are set to be parallel to the direction of the C_3 axis of $[M(H_2O)_6]^{2+}$ and to be perpendicular to z_P of D1, respectively. The magnetic and the geometric parameters of $[M(H_2O)_6][SiF_6]$ used for spectral simulation are shown in Table 1. The geometrical parameters were calculated using the results of diffraction methods.[36−38] The paramagnetic shift and spin−spin relaxation due to the dipolar interaction between the deuteron and the paramagnetic ions are calculated using metal ions in 3^3 hexagonal unit cells (81 metal ions). The numerical efficiency for the calculation of the time evolution of the magnetization was confirmed using several n_{rot} values. For the spectral simulation in the present work, $n_{\mathrm{rot}} = 200$ was used.

4. Results and Discussion

In order to characterize the paramagnetic effects, we first measured the ^{2}H MAS NMR spectra of diamagnetic $[Zn(H_2O)_6]$-

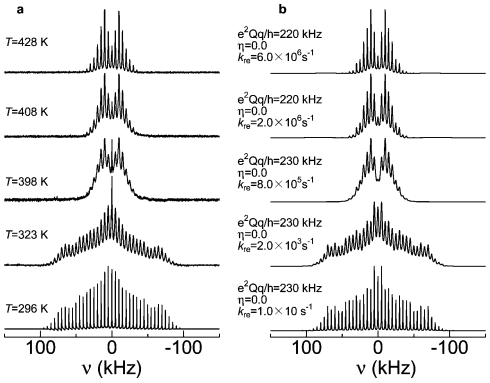

Figure 2. Temperature dependence of ^{2}H MAS NMR spectra for diamagnetic $[Zn(H_2O)_6][SiF_6]$. Observed (a) and simulated (b) spectra.

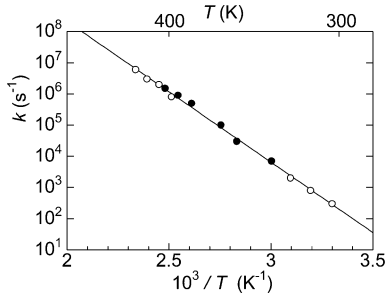

Figure 3. Temperature dependence of the jumping rate (k_{re}) for the three-site jump of $[Zn(H_2O)_6]^{2+}$ about the C_3 axis. Open and closed circles show k_{re} obtained by ^{2}H NMR MAS spectra and broadline spectra, respectively.

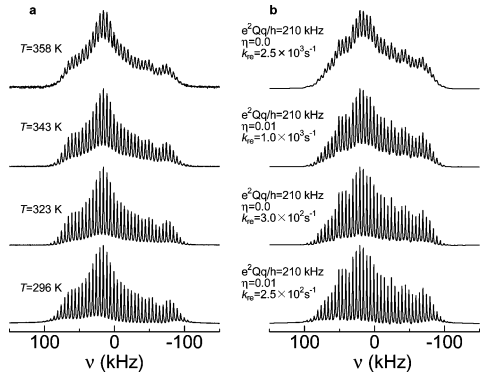

Figure 4. Temperature dependence of ^{2}H MAS NMR spectra for paramagnetic $[Ni(H_2O)_6][SiF_6]$ in the temperature range of 296−358 K. Observed (a) and simulated (b) spectra.

$[SiF_6]$. The temperature dependence of the ^{2}H MAS NMR spectrum of $[Zn(H_2O)_6][SiF_6]$ above room temperature is shown in Figure 2. The ^{2}H MAS NMR spectra were measured at a spinning speed of 5 kHz. $[Zn(H_2O)_6]^{2+}$ in $[Zn(H_2O)_6][SiF_6]$ exhibits two types of molecular motions: a 180° flip of water molecules and a three-site jump of $[Zn(H_2O)_6]^{2+}$ about its C_3 axis. From the shape of the spinning sideband pattern, in this temperature range, the electric field gradient (EFG) at the ^{2}H nucleus is averaged by the fast 180° flip of water molecules, and the temperature variation of the ^{2}H MAS NMR spectrum can be explained by the three-site jump of $[Zn(H_2O)_6]^{2+}$. The broadline ^{2}H NMR spectrum was sensitive to the three-site jump of $[Zn(H_2O)_6]^{2+}$ about its C_3 axis above 333 K (see Supporting Information) and to the 180° flip of water molecules below 203 K. From the results of the broadline

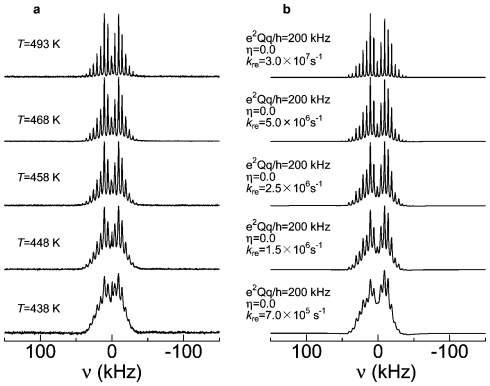

Figure 5. Temperature dependence of ^{2}H MAS NMR spectra for paramagnetic $[Ni(H_2O)_6][SiF_6]$ in the temperature range of 438−493 K. Observed (a) and simulated (b) spectra.

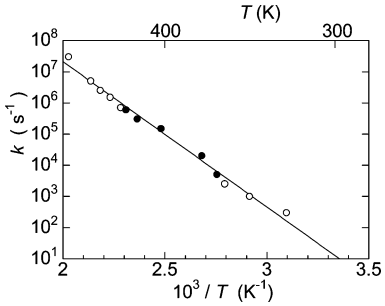

Figure 6. Temperature dependence of the jumping rate (k_{re}) for the three-site jump of $[Ni(H_2O)_6]^{2+}$ about the C_3 axis. Open and closed circles show k_{re} obtained by ^{2}H NMR broadline spectra[17] and MAS spectra, respectively.

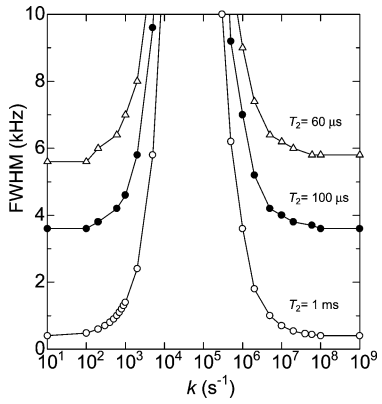

Figure 7. Dependence of full width at half-maximum (fwhm) of spinning sideband on jumping rate k_{re}. Open circle, closed circle, and open triangle are results of calculations for angular-averaged $T_2 = 1$ ms, 100 us, and 60 us, respectively.

^{2}H NMR spectrum, the rates of the 180° flip of water molecules and the three-site jump of $[Zn(H_2O)_6]^{2+}$ are predicted to be $k_{H_2O} > 10^9$ s^{-1} and $k_{re} < 10^2$ s^{-1} at 293 K, respectively. So, these molecular motions do not induce linebroadening of the ^{2}H MAS NMR spectrum at 296 K. The isotropic spin−spin relaxation time T_2 of 1.0 ms, which was obtained from the full width at half-maximum (fwhm) of spinning sideband (0.32 kHz) at 296 K, was used for whole spectral simulation of $[Zn(H_2O)_6][SiF_6]$ as the homogeneous line width. Figure 2b represents the spectral simulation assuming the 180° flip of water molecules and the three-site jump of $[Zn(H_2O)_6]^{2+}$. For the 180° flip of water molecules, a constant

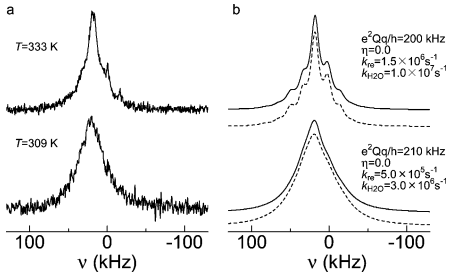

Figure 8. (a) Experimental ^{2}H MAS NMR spectra for paramagnetic $[Mn(H_2O)_6][SiF_6]$ at 309 and 333 K. (b) Calculated ^{2}H MAS NMR spectra. Solid lines show the spectra without DFS. Broken lines show the spectra including DFS.

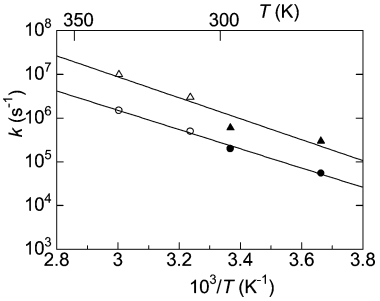

Figure 9. Temperature dependence of the jumping rates for the three-site jump of $[Mn(H_2O)_6]^{2+}$ about the C_3 axis (k_{re}) and the 180° flip of water molecules (k_{H_2O}). Closed circles and triangles show k_{re} and k_{H2O} obtained by ^{2}H NMR broadline spectra.[19] Open circles and triangles show k_{re} and k_{H2O} obtained by ^{2}H NMR MAS spectra, respectively.

k_{H_2O} value ($= 1.0 \times 10^9$ s^{-1}) was used. The temperature dependence of the rate k_{re} for the three-site jump of $[Zn(H_2O)_6]^{2+}$ about its C_3 axis obtained from the ^{2}H NMR broadline and MAS spectra is shown in Figure 3. The ^{2}H MAS NMR spectra provided information about the three-site jump of $[Zn(H_2O)_6]^{2+}$ in the dynamic ranges of $k_{re} \geq 5 \times 10^6$ s^{-1} and $k_{re} \leq 10^3$ s^{-1}, which were undetectable in the ^{2}H NMR broadline spectra. From the gradient of the log(k_{re}) versus T^{-1} plots, the activation energy of the three-site jump of $[Zn(H_2O)_6]^{2+}$ was obtained as 83 kJ mol^{-1}.

For $[Ni(H_2O)_6][SiF_6]$, Ni^{2+} possesses the spin state of $S = 1$ and isotropic g-factor ($g = 2.26$).[39,40] Figures 4 and 5 show the ^{2}H MAS NMR spectra of $[Ni(H_2O)_6][SiF_6]$ observed in the temperature ranges 296−358 K and 438−493 K, respectively. The ^{2}H MAS NMR spectra were measured at a spinning speed of 5 kHz. The spectra showed an asymmetric line shape due to the paramagnetic shift caused by the dipolar interaction between the ^{2}H nuclei and the Ni^{2+}. The shape of the spinning sideband pattern at 296 K indicates that the electric field gradient (EFG) at the ^{2}H nucleus is averaged by the fast 180° flip of water molecules. The fwhm of the spinning sideband of $[Ni(H_2O)_6][SiF_6]$ was 1.1 kHz at 296 K. From the observed T_1 value,[17] the τ_e and the angular-averaged T_2 values were obtained as 6.0×10^{-11} s and 500 μs, respectively. Using this T_2 value, fwhm due to the spin−spin relaxation which is caused by the dipolar interaction between the ^{2}H nuclei and the Ni^{2+} was estimated as 0.6 kHz at 296 K. Therefore, the line width of the spinning sideband at 296 K is found to be dominated by the three-site jump of $[Ni(H_2O)_6]^{2+}$ about its C_3 axis. The temperature variation of the ^{2}H MAS NMR spectrum was simulated by changing the jumping rate of the three-site jump of $[Ni(H_2O)_6]^{2+}$ about its C_3 axis. Figures 4b and 5b show the spectral simulation assuming the 180° flip of water molecules and the three-site jump of $[Ni(H_2O)_6]^{2+}$. For the 180° flip of water molecules, a constant k_{H_2O} value ($= 1.0 \times 10^9$ s^{-1}) was used. The linebroadening due to anisotropic spin−spin relaxation which is caused by the dipolar interaction between the ^{2}H nuclei and the Ni^{2+} was estimated using eq 9 and τ_e obtained from the observed T_1 value at each temperature.[17] The paramagnetic shift ν_D due to the electron−deuteron dipolar coupling for the nearest Ni^{2+} and the next nearest Ni^{2+} were estimated from eq 5 as 38 and 9 kHz for D1 and 45 and 6 kHz for D2 at 296 K and 23 and 5 kHz for D1 and 27 and 4 kHz for D2 at 493 K. Figure 6 shows the temperature dependence of the rate k_{re} for the three-site jump of $[Ni(H_2O)_6]^{2+}$ about its C_3 axis obtained by the ^{2}H NMR MAS and broadline spectra. k_{re} in the range of 10^3-10^6 s^{-1} were obtained by the ^{2}H NMR broadline spectra.[17] On the contrary, the ^{2}H MAS NMR spectra of $[Ni(H_2O)_6][SiF_6]$ provided information of molecular motion in the dynamic range of 10^5 s$^{-1} \leq k_{re} \leq 10^7$ s^{-1} and 10^2 s$^{-1} \leq k_{re} \leq 10^3$ s^{-1}. From the gradient of the log(k_{re}) versus T^{-1} plots, the activation energy of the three-site jump of $[Ni(H_2O)_6]^{2+}$ was obtained as 89 kJ mol^{-1}.

The influences of anisotropic spin−spin relaxation due to the electron−deuteron dipolar coupling and molecular motion to linebroadening of spinning sideband in the ^{2}H MAS NMR spectrum were investigated by spectral simulation using the geometrical and the magnetic parameters of $[Ni(H_2O)_6][SiF_6]$. Fwhm of the spinning sideband was obtained by simulation of the ^{2}H MAS NMR spectra at a spinning speed of 20 kHz. Figure 7 shows the dependence of fwhm on the jumping rate k_{re} of $[Ni(H_2O)_6]^{2+}$ about its C_3 axis for different spin−spin relaxation rates. The spin−spin relaxation rate was altered by changing the τ_e values in eq 9. The angular-averaged $T_2 (= 1/R^i_{2p})$ value is shown in Figure 7. A constant k_{H_2O} value ($=1.0 \times 10^9$ s^{-1}) was used for the simulation. Although fwhm increases with decreasing T_2, linebroadening of a spinning sideband due to the molecular motion appears in the similar dynamic range of 10^2 s$^{-1} \leq k_{re} \leq 10^8$ s^{-1}. These results suggest that information of molecular motion can be obtained from the ^{2}H MAS NMR spectrum using fast sample spinning even for the samples with a fast spin−spin relaxation process between the electron and the deuteron.

For $[Mn(H_2O)_6][SiF_6]$, the g-factor of Mn^{2+} is isotropic ($g = 2.00$).[41,42] Mn^{2+} possesses a larger spin quantum number ($S = 5/2$) and a longer correlation time of electron spin ($\tau_e \sim 3 \times 10^{-10}$ s) than those of other transition metals in the $[M(H_2O)_6]^{2+}$ type complex ions.[16−19] So, ^{2}H NMR T_2 becomes very short ($\sim$60 μs), and fast sample spinning speed is required for the measurements of ^{2}H MAS NMR spectra of $[Mn(H_2O)_6][SiF_6]$. Hence, the measurements of ^{2}H MAS NMR spectra of $[Mn(H_2O)_6][SiF_6]$ were performed at a spinning speed of 16 kHz. The ^{2}H MAS NMR spectra of $[Mn(H_2O)_6][SiF_6]$ observed at 309 and 333 K are shown in Figure 8. Because of dehydration, we could not obtain the ^{2}H MAS NMR spectra of $[Mn(H_2O)_6][SiF_6]$ at a temperature higher than 333 K. The broadening of the spectrum is caused by the molecular motion and the paramagnetic spin−spin relaxation. The spectrum at 333 K was slightly narrower than that at 303 K and exhibited the structure because of the spinning sideband. From τ_e estimated using the T_1 values, the contribution of the paramagnetic spin−spin relaxation to the line width of the spinning sideband becomes $\sim$5.3 kHz and is almost temperature-independent in this temperature range.[18] Therefore, the narrowing of the spectrum can be attributed to the molecular motions. Figure 8b shows the spectral simulation including the paramagnetic shift and the spin−spin relaxation due to the dipolar interaction between the ^{2}H nuclei and the Mn^{2+} in the presence of the 180° flip of water molecules and the three-site jump of

$[Mn(H_2O)_6]^{2+}$. The dipolar coupling ν_D for the nearest Mn^{2+} to D1 at 309 and 333 K are 173 and 157 kHz, and ν_D for the next nearest Mn^{2+} to D1 at 309 and 333 K are 37 and 34 kHz. ν_D for the nearest Mn^{2+} to D2 at 309 and 333 K are 161 and 147 kHz, and ν_D for the next nearest Mn^{2+} to D2 at 309 and 333 K are 26 and 23 kHz. The anisotropic spin−spin relaxation rates were calculated using $\tau_e = 3.0 \times 10^{-10}$ s for eq 9.[18] When the broadening of the linewidths are caused by the fast paramagnetic transverse relaxation, then the dynamic frequency shift (DFS), the imaginary part of the spectral density, contributes to the shift in the resonance frequency.[31] DFS in the ^2H NMR frequency due to the paramagnetic dipolar interaction is given by

$$\delta^i_{\mathrm{DFS}}(t) = \frac{4}{3}\left(\frac{\mu_0}{4\pi}\right)^2 \gamma_D^2 \mu_B^2 S(S+1) \sum_j g_j^2(t) \times \left\{\frac{1}{6}\left|A^{ij}_{20}(t)\right|^2 \left(\frac{(\omega_N - \omega_e)\tau_e^2}{1+(\omega_N-\omega_e)^2\tau_e^2}\right) + \frac{1}{2}\left|A^{ij}_{21}(t)\right|^2 \left(\frac{2\omega_e\tau_e^2}{1+\omega e_2\tau_e^2} + \frac{\omega_N\tau_e^2}{1+\omega_N^2\tau_e^2}\right) + \left|A^{ij}_{22}(t)\right|^2 \frac{(\omega_N+\omega_e)\tau_e^2}{1+(\omega_N+\omega_e)^2\tau_e^2}\right\} \quad (23)$$

The angular-averaged DFS value was estimated as 1.0 kHz for the ^2H NMR spectrum of $[Mn(H_2O)_6][SiF_6]$. In order to investigate the effects of DFS to the ^2H MAS NMR spectrum, the spectral simulation including $\delta^i_{\mathrm{DFS}}(t)$ in eq 1 was performed. The broken lines in Figure 8b show the spectral simulation including the anisotropic DFS. As can be seen from this figure, the apparent variation in the ^2H MAS NMR spectrum due to DFS was not recognized. The jumping rates for the 180° flip of water molecules (k_{H_2O}) and the three-site jump of $[Mn(H_2O)_6]^{2+}$ (k_{re}) were obtained from the spectral simulation. Figure 9 shows the temperature dependences of k_{H_2O} and k_{re} obtained from ^2H NMR MAS spectra and broadline spectra. The ^2H NMR MAS spectrum was effective above 300 K, and the broadline spectrum was effective below 300 K for the studies of molecular dynamics in $[Mn(H_2O)_6][SiF_6]$. From the gradient of the log(k) versus T^{-1} plots, the activation energies of the 180° flip of water molecule and the three-site jump of $[Mn(H_2O)_6]^{2+}$ were obtained as 45 and 42 kJ mol^{-1}, respectively.

The spin state of Co^{2+} in $[Co(H_2O)_6][SiF_6]$ is presented by a fictitious spin = 1/2, and the g-factor of Co^{2+} is anisotropic.[42−44] Figure 10a shows the ^2H MAS NMR spectrum of $[Co(H_2O)_6][SiF_6]$ observed at 293 K. The spectrum was measured at a spinning speed of 5 kHz. The correlation time of the electron spin at 293 K was obtained as $\tau_e = 2.0 \times 10^{-12}$ s from the results of ^2H NMR T_1,[16] and the contribution of the paramagnetic spin−spin relaxation to the line width of the spinning sideband was estimated as 0.03 kHz. The ^2H NMR broadline spectra were sensitive to the three-site jump of $[Co(H_2O)_6]^{2+}$ and the 180° flip of water molecule in the temperature ranges of 303−393 and 163−243 K, respectively. From the results of the ^2H NMR broadline spectra, the jumping rates for the 180° flip of water molecules and the three-site jump of $[Co(H_2O)_6]^{2+}$ at 293 K are predicted to be $k_{H_2O} = 2 \times 10^9$ s^{-1} and $k_{re} = 8 \times 10^2$ s^{-1}, respectively.[16] The effects of the anisotropic g-factor on ^2H MAS NMR spectra were investigated from the spectral simulation using these values. Figure 10b,c shows the simulation spectra

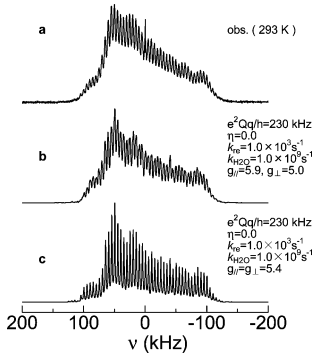

Figure 10. (a) Observed ^2H MAS NMR spectrum for paramagnetic $[Co(H_2O)_6][SiF_6]$ at 293 K. Simulated spectra using (b) anisotropic and (c) isotropic g factors.

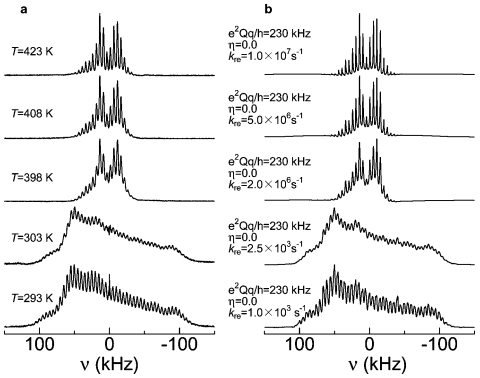

Figure 11. Temperature dependence of ^2H MAS NMR spectra for paramagnetic $[Co(H_2O)_6][SiF_6]$ in the temperature range of 293−423 K. Observed (a) and simulated (b) spectra.

using the anisotropic g-factor ($g_{||} = 5.9$, $g_\perp = 5.0$) and the isotropic g-value ($g_{iso} = 5.4$), respectively. The observed spectra were highly reproducible by former simulation. The anisotropy of the g-factor induces the broadening and the structure of the spinning sideband. This result suggests that an estimation of the effects of the anisotropic g-factor on the spinning sideband is important for the analysis of molecular motions using a ^2H MAS NMR spectrum. From the experiments of the susceptibilities, $g_{||} = 5.98$ and $g_\perp = 3.37$ at 290.4 K have been reported.[43] Anisotropy of the g-factor observed in the ^2H MAS NMR spectra of $[Co(H_2O)_6][SiF_6]$ is fairly reduced as compared with that observed by the susceptibilities. Similar phenomena have been reported for other compounds.[29] These results might be caused by the delocalization of unpaired electron spin of Co^{2+}. The temperature dependence of the ^2H MAS NMR spectrum of $[Co(H_2O)_6][SiF_6]$ at a spinning speed of 5 kHz is shown in Figure 11. Figure 11b shows the spectral simulation assuming the 180° flip of water molecules and the three-site jump of $[Co(H_2O)_6]^{2+}$. For the 180° flip of water molecules, a constant k_{H_2O} value ($= 1.0 \times 10^9$ s^{-1}) was used. The linebroadening due to anisotropic spin−spin relaxation which is caused by the dipolar interaction between the ^2H nuclei and the Co^{2+} was estimated using eq 9 and τ_e obtained from the observed T_1 value at each temperature.[16] The paramagnetic shifts due to the electron−deuteron dipolar coupling for the nearest Co^{2+} were estimated as $\nu_{D||} = 88$ kHz and $\nu_{D\perp} = 63$ kHz for D1 and $\nu_{D||} = 99$ kHz and $\nu_{D\perp} = 71$ kHz for D2 at 296 K and $\nu_{D||} = 62$ kHz and $\nu_{D\perp} = 45$ kHz for D1 and $\nu_{D||} = 70$ kHz and $\nu_{D\perp} = 50$ kHz for D2 at 413 K. Figure 12 shows the temperature dependence of the rate k_{re} for the three-site jump of $[Co(H_2O)_6]^{2+}$ about its C_3 axis obtained by ^2H NMR MAS and broadline spectra. The information of molecular motion in the dynamic range of 10^6

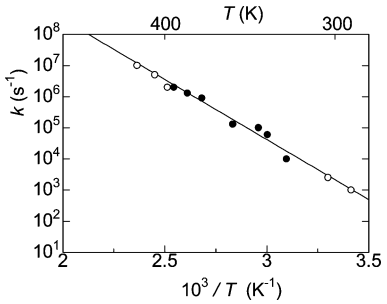

Figure 12. Temperature dependence of the jumping rate (k_{re}) for the three-site jump of $[Co(H_2O)_6]^{2+}$ about the C_3 axis. Open and closed circles show k_{re} obtained by ^2H NMR broadline spectra[16] and MAS spectra, respectively.

$s^{-1} \leq k$ was obtained from the ^2H MAS NMR spectrum even for the compound with an anisotropic g-factor. From the gradient of the $\log(k_{re})$ versus T^{-1} plots, the activation energies of the three-site jump of $[Co(H_2O)_6]^{2+}$ was obtained as 74 kJ mol^{-1}.

5. Conclusion

We demonstrated the ^2H MAS NMR spectral simulation including the effects of paramagnetic shift, anisotropic g-factor, and anisotropic spin−spin relaxation due to the dipolar interaction between the deuteron and the paramagnetic ions in the presence of the molecular motion using not only the nearest paramagnetic ion but also the distant ones. In the ^2H MAS NMR spectrum of the paramagnetic compounds, the anisotropy of the g-factor and the fast spin−spin relaxation due to the dipolar interaction between the deuteron and the paramagnetic ions, as well as molecular motion, have a large effect on the line width of the spinning sideband. The analysis, which takes into account these effects, makes it possible to obtain information of the molecular motion in the dynamic range of 10^2 $s^{-1} \leq k \leq 10^8$ s^{-1} even for paramagnetic compounds. The activation energies of the three-site jump of $[M(H_2O)_6]^{2+}$ (Ni^{2+} = 89 kJ mol^{-1}, Zn^{2+} = 83 kJ mol^{-1}, Co^{2+} = 74 kJ mol^{-1}, and Mn^{2+} = 42 kJ mol^{-1}) were obtained by the analysis of ^2H NMR spectra. We have pointed out that the structure of $[M(H_2O)_6]^{2+}$ elongated along the C_3 axis makes the activation energy small.[16,17] The activation energies of the three-site jump of $[M(H_2O)_6]^{2+}$ obtained by this study reflected the degree of the elongation of $[M(H_2O)_6]^{2+}$.

Acknowledgment. This work was supported by a Grant-In-Aid for Science Research in a Priority Area " Chemistry of Coordination Space" (No. 434) and a Grant-In-Aid for Scientific Research (No. 19510103) from the Ministry of Education, Culture, Sports, Science and Technology, Government of Japan.

Supporting Information Available: Temperature dependence of ^2H NMR broadline spectra for $[Zn(H_2O)_6][SiF_6]$. This material is available free of charge via the Internet at http://pubs.acs.org.

References and Notes

(1) Schmidt-Rohr, K.; Spiess, H. W. In *Multidimensional Solid-State NMR and Polymers*; Academic Press: London, 1994.

(2) Vold, R. R. In *Nuclear Magnetic Resonance Probes of Molecular Dynamics*; Tycko, R., Ed.; Kluwer Academic Publishers: Norwell, MA, 1994; pp 27−112.

(3) Vold, R. R.; Vold, R. L. In *Advances in Magnetic and Optical Resonance, Vol. 16*; Warren, W. S., Ed.; Academic Press Inc: San Diego, 1991; pp 85−171.

(4) Hiyama, Y.; Silverton, J. V.; Torchia, D. A.; Gerig, J. T.; Hammond, S. J. *J. Am. Chem. Soc.* **1986**, *108*, 2715.

(5) Greenfield, M. S.; Ronemus, A. D.; Vold, R. L.; Vold, R. R.; Ellis, P. D.; Raidy, T. E. *J. Magn. Reson.* **1987**, *72*, 89.

(6) Wittebort, R. J.; Olejniczak, E. T.; Griffin, R. G. *J. Chem. Phys.* **1987**, *86*, 5411.

(7) Long, J. R.; Ebelhauser, R.; Griffin, R. G. *J. Phys. Chem. A* **1997**, *101*, 988.

(8) Kimura, J.; Fukase, T.; Mizuno, M.; Suhara, M. *Z. Naturforsch.* **1998**, *53a*, 453.

(9) Iijima, T.; Mizuno, M.; Suhara, M.; Endo, K. *Z. Naturforsch.* **2002**, *57a*, 408.

(10) Iijima, T.; Mizuno, M. *Chem. Phys. Lett.* **2003**, *380*, 736.

(11) Siminovitch, D. J.; Rance, M.; Jeffrey, K. R.; Brown, M. F. *J. Magn. Reson.* **1984**, *58*, 62.

(12) Antonijevic, S.; Wimperis, S. *J. Magn. Reson.* **2003**, *164*, 343.

(13) Lin, T.-H.; Di Natale, J. A.; Vold, R. R. *J. Am. Chem. Soc.* **1994**, *116*, 2133.

(14) Iijima, T.; Orii, K.; Mizuno, M.; Suhara, M. *Z. Naturforsch.* **1998**, *53a*, 447.

(15) Mizuno, M.; Hamada, Y.; Kitahara, T.; Suhara, M. *J. Phys. Chem. A* **1999**, *103*, 4981.

(16) Iijima, T.; Mizuno, M.; Suhara, M. *Z. Naturforsch.* **2000**, *55a*, 173.

(17) Mizuno, M.; Iijima, T.; Suhara, M. *J. Phys.: Condens. Matter* **2000**, *12*, 7261.

(18) Iijima, T.; Mizuno, M.; Hamada, K.; Suhara, M.; Endo, K. *J. Phys. Chem. Solids* **2005**, *66*, 1101.

(19) Mizuno, M.; Itakura, N.; Endo, K. *Chem. Phys. Lett.* **2005**, *416*, 358.

(20) Suwelack, D.; Rothwell, W. P.; Waugh, J. S. *J. Chem. Phys.* **1980**, *73*, 2559.

(21) Schmidt, A.; Vega, S. *J. Chem. Phys.* **1987**, *87*, 6895.

(22) Vega, S. In *Nuclear Magnetic Resonance Probes of Molecular Dynamics;* Tycko, R., Ed.; Kluwer Academic Publishers: Norwell, MA, 1994; pp 155−222.

(23) Hologne, M.; Hirschinger, J. *Solid State Nucl. Magn. Reson.* **2003**, *26*, 1.

(24) Duer, M. J.; Levitt, M. H. *Solid State Nucl. Magn. Reson.* **1992**, *1*, 211.

(25) Kristensen, J. H.; Bildsøe, H.; Jakobsen, H. J.; Nielsen, N. C. *J. Magn. Reson.* **1992**, *100*, 437.

(26) Heaton, N. J. *Mol. Phys.* **1997**, *92*, 251.

(27) Kristensen, K. H.; Hoatson, G. L.; Vold, R. L. *Solid State Nucl. Magn. Reson.* **1998**, *13*, 1.

(28) Soda, G.; Chiba, T. *J. Chem. Phys.* **1969**, *50*, 439.

(29) Lee, H.; Polenova, T.; Beer, R. H.; McDermott, A. E. *J. Am. Chem. Soc.* **1999**, *121*, 6884.

(30) Lee, H.; Ortiz de Montellano, P. R.; McDermott, A. E. *Biochemistry* **1999**, *38*, 10808.

(31) Werbelow, L. G In *Encyclopedia of Nuclear Magnetic Resonance, Vol. 6*; Grant, D. M., Harris, R. K., Eds.; Wiley: London, 1996; pp 4072−4078.

(32) Smith, B. T.; Boyle, J. M.; Garbow, B. S.; Ikebe, Y.; Klema, V. C; Moler, C. B. *Matrix Eigensystem Routines: Eispack Guide*; Springer-Verlag: Berlin, 1976.

(33) Rose, M. E. *Elementary Theory of Angular Momentum*; Wiley: New York, 1957.

(34) Bloom, M.; Davis, J. H.; Valic, M. I. *Can. J. Phys.* **1980**, *58*, 1510.

(35) Barbara, T. M.; Greenfield, M. S.; Vold, R. L.; Vold, R. R. *J. Magn. Reson.* **1986**, *69*, 311.

(36) Ray, S.; Zalkin, A.; Templeton, D. H. *Acta Crystallogr., Sect. B* **1973**, *29*, 2741.

(37) Chevrier, G.; Saint-James, R. *Acta Crystallogr., Sect. C* **1990**, *46*, 186.

(38) Chevrier, G. *Acta Crystallogr., Sect. B* **1991**, *47*, 224.

(39) Rubins, R. S.; Clark, J. D.; Jani, S. K. *J. Chem. Phys.* **1977**, *67*, 893.

(40) Peng, L. C.; Wu, P. F.; Zhou, K. W. *Phys. Status Solidi* **1996**, *195*, 569.

(41) Bleaney, B.; Ingram, D. J. E. *Proc. R. Soc. London, Ser. A* **1951**, *205*, 336.

(42) Abragam, A.; Bleaney, B. *Electron Paramagnetic Resonance of Transition Ions*; Clarendon: Oxford, 1970.

(43) Bose, A.; Jackson, L. C.; Rai, R. *Ind. J. Phys.* **1965**, *39*, 7.

(44) Majumdar, M.; Datta, S. K. *J. Chem. Phys.* **1965**, *42*, 418.